Int. J. Electrochem. Sci., 16 **(2021)** Article ID: 210349, doi: 10.20964/2021.03.26

International Journal of
ELECTROCHEMICAL
SCIENCE
www.electrochemsci.org

Influence of Polyvinyl Pyrrolidone (PVP) on Vanadium-based Compound Composite Performances for Aqueous Zinc-Ion Batteries

Shijia Li[1], *Liping Qin*[1,*], *Lijun Li*[1,2,*], *Hao Cheng*[1,2], *Guozhao Fang*[3], *Qi Zhu*[1]

[1] Guangxi Key Laboratory of Green Processing of Sugar Resources, College of Biological and Chemical Engineering, Guangxi University of Science and Technology, Liuzhou 545006, Guangxi, P.R. China
[2] Province and Ministry Co-sponsored Collaborative Innovation Center of Sugarcane and Sugar Industry, Nanning 530004, Guangxi, P.R. China
[3] School of Materials Science and Engineering, Central South University, Changsha 410083, Hunan, P.R. China
[*]E-mail: qinlp2005@126.com (L.P. Qin), gxustllj@163.com (L.J. Li)

Received: 25 October 2020 / *Accepted:* 19 December 2020 / *Published:* 31 January 2021

Aqueous zinc-ion rechargeable batteries are potential candidates that are widely used in large-scale energy storage fields owing to their high safety, acceptable energy density, and low cost. However, the strong electrostatic interaction between divalent Zn^{2+} and the host lattice leads to slow reaction kinetics and poor reversibility of Zn^{2+} insertion/extraction. In this study, vanadium-based compound composites with the main phase of $Zn_2V_2O_7$ consisting of ZnV_2O_6 and ZnV_2O_4 was synthesised by a simple hydrothermal method using polyvinyl pyrrolidone (PVP) as a surfactant to adjust the morphology. Meanwhile, PVP molecules cause a change in the coordination environment of atoms in the crystal lattice of the samples and reduce the high-valence state of V to the low-valence state, forming a hybrid valence, which is beneficial to the multi-step reaction of vanadium. As expected, the vanadium-based compound composite displays an initial discharge capacity of 386 mA h g^{-1} at 300 mA g^{-1} and a discharge capacity of 114 mA h g^{-1} at 3 A g^{-1} with 64% reversible capacity after 4000 cycles, exhibiting good long-term cycle life. The excellent electrochemical performance of vanadium-based compounds is due to the good dispersion and hybrid valence, which contributes to the high ion-diffusion coefficient as well as to the deep insertion and extraction of Zn^{2+}.

Keywords: vanadium-based compounds composite; cathode; aqueous zinc-ion batteries; electrochemical performance

1. INTRODUCTION

Lithium-ion batteries have successfully played a vital role in the fields of electric vehicles and portable electronic devices owing to their high energy density and long cycle life. However, the safety, cost, and serious environmental problems of lithium batteries cannot meet the requirements for scale energy storage devices, prompting the development of alternative systems [1-7]. In this case, many aqueous rechargeable batteries based on multivalent metal ions such as Mg^{2+}, Al^{3+}, and Zn^{2+} batteries have been studied for grid-scale electrochemical energy storage owing to their safety and high storage capacity derived from their polyvalent cations and related multi-electron transfer reactions. Among these aqueous rechargeable batteries, zinc-ion batteries (ZIBs) have gained the highest interest owing to their favourable properties of high theoretical specific capacity (820 mA h g^{-1}, 5855 mA h cm^{-3}), low redox potential (−0.76 V vs. standard hydrogen electrode), mild neutral pH electrolyte, and high chemical stability in waterr [8, 9].

As an important part of the aqueous zinc-ion battery system, cathode materials with outstanding performance have been developed. Currently, various types of electrode materials such as vanadium-based materials [10], manganese-based materials [11] and Prussian blue analogues [12] have been successfully used as cathodes for aqueous ZIBs [13, 14]. Vanadium-based compound materials are notable among cathode materials owing to their various structures, large layer spacing, high specific capacity, and various valence states of vanadium. A variety of vanadium-based compounds such as V_2O_5 [15, 16], metal-ion-preintercalated V_2O_5 [17-19], and sodium vanadate [20-22] have been studied as cathode materials for ZIBs. In addition to the above vanadium-based compounds, Alshareef et al. synthesised $Zn_3V^{5+}{}_2O_7(OH)_2{\cdot}2H_2O$ nanowires using a microwave approach. The $Zn_3V^{5+}{}_2O_7(OH)_2{\cdot}2H_2O$ cathode demonstrated capacities of 213 and 76 mA h g^{-1} at current densities of 50 and 3 A g^{-1}, respectively, and a capacity retention of 68% at 200 mA g^{-1} over 300 cycles was demonstrated [23]. Sambandam et al. synthesised α-$Zn_2V^{5+}{}_2O_7$ with a layered structure consisting of tetrahedrally coordinated VO_4 and trigonal bipyramid ZnO_5 polyhedra; it delivered an average capacity of 220 mAh g^{-1}, and 81% capacity retention was maintained at 4 A g^{-1} over 1000 cycles [24]. Fang et al. demonstrated spinel ZnV_2O_4 nanoparticles as a high-capacity cathode material for aqueous ZIBs [25]. The cathode material exhibited 82.4% capacity retention over 1000 cycles with a remaining reversible capacity of 206 mA h g^{-1}. By adjusting the morphology, pre-intercalating metal ions or H_2O molecules, and coating carbon layers and metal oxides, the electrochemical performance of vanadium-based compounds has been greatly improved. However, the capacity and cycling stability are still not satisfactory. These materials suffer from strong electrostatic interactions with divalent Zn^{2+}, which can cause sluggish reaction kinetics and inhibit reversible Zn^{2+} storage. In fact, the electrochemical performance of batteries is highly dependent on the inherent phase categories, structure and surface characteristics of electrode materials. Enlarging the ion transport pathway, constructing atomic vacancies, improving the ion diffusion coefficient and inducing the surface pseudocapacitive effect are effective ways to overcome the above shortcomings. Thus, it is necessary to enhance the zinc ion storage kinetics of vanadium-based compound materials using combination of these methods.

Herein, the vanadium-based compound composites consisting of $Zn_2V_2O_7$, ZnV_2O_6, and ZnV_2O_4 are prepared via a facile hydrothermal route and investigated as the cathode material for ZIBs. Moreover, in order to optimise the performance of the cathode materials, different contents of polyvinyl pyrrolidone (PVP) are added during the synthesis to adjust the morphology and structure of the samples. The results indicate that PVP molecules cause the phase change of samples, improve dispersion, and reduce the high-valence state of V to the low-valence state. The good dispersion and hybrid valence of the vanadium-based compound composite are helpful for the electrochemical performance improvement.

2. EXPERIMENTAL

2.1 Materials preparation

Typically, 0.464 g $Zn(NO_3)_2{\cdot}6H_2O$, 0.364 g V_2O_5, and 0.1 g PVP were added to 40 mL deionised (DI) water under vigorous stirring for 2 h. Then, the obtained orange dispersion was transferred into a 50 mL Teflon-lined stainless-steel autoclave and maintained at 250 °C for 24 h. The obtained precipitate was washed with DI water and ethanol, and then dried at 80 °C for 12 h. Finally, a green powder was obtained. For comparison, 0 and 0.2 g of PVP were added during the mixing process with other parameters unaltered. The composites with different amounts of added PVP (0 g, 0.1 g, 0.2 g) were designated as ZVO, ZVO-0.1P, and ZVO-0.2P, respectively.

2.2 Characterizations

The crystal structure and phase of the prepared samples were analysed using a Bruker D8A-A25 X-ray diffractometer with K_α X-ray of the Cu target as the excitation source. The morphology of the samples was characterised using cold field emission scanning electron microscopy (SEM; Hitachi S-4800) and high-resolution transmission electron microscopy (TEM; JEOL JEM-2100). The valence states of the elements were analysed using X-ray photoelectron spectrometer (XPS; Thermo Scientific ESCALAB 250Xi).

2.3 Electrochemical measurements

To evaluate the electrochemical capability, CR2016 coin-type batteries were constructed using the obtained ZVO, ZVO-0.1P, and ZVO-0.2P samples as the cathode material. Zinc foil with a thickness of 0.2 mm was used as the anode, Whatman grade glass fibre was used as the separator, and a 2 mol L^{-1} $ZnSO_4$ solution was used as the electrolyte. The cathode electrode was prepared by pressing a slurry consisting of 70% active material, 20% conductive carbon, and 10% PVDF binder onto a stainless-steel mesh, and then drying the slurry at 60 °C for 12 h. The cells were assembled and tested at room temperature. The galvanostatic charge/discharge measurements were performed in the voltage range of 0.4–1.8 V using a CT2001A Land Battery system (Wuhan, China). Cyclic

voltammetry (CV) was carried out using a CHI 660b electrochemical workstation (Shanghai, Chenhua).

3. RESULTS AND DISCUSSION

Fig. 1a shows the XRD patterns of ZVO, ZVO-0.1P, and ZVO-0.2P. It can be clearly seen that the three samples are all mixed phases composed of monoclinic $Zn_2V_2O_7$ (PDF 70–1532), monoclinic ZnV_2O_6 (PDF 23–0757), and cubic ZnV_2O_4 (PDF No. 65–3108). When PVP is 0 g, the main phase of the ZVO sample is the composite of $Zn_2V_2O_7$ and ZnV_2O_6 with a low-intensity diffraction peak of ZnV_2O_4. When PVP is 0.1 g, the main phase of the composite is $Zn_2V_2O_7$ with a small number of low-intensity diffraction peaks belonging to ZnV_2O_6 and ZnV_2O_4.

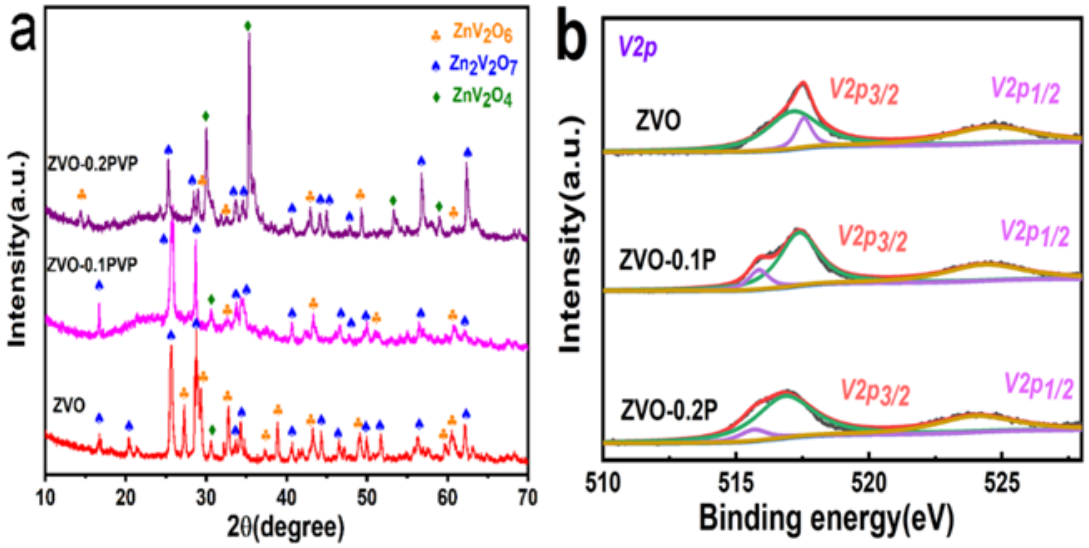

Figure 1. (a) XRD patterns of ZVO, ZVO-0.1P, and ZVO-0.2P. (b) V 2p peaks in XPS profile of ZVO, ZVO-0.1P, and ZVO-0.2P.

When the amount of PVP is increased to 0.2 g, the number and intensity of the ZnV_2O_4 diffraction peaks rapidly increase, while the intensity of the $Zn_2V_2O_7$ diffraction peaks decrease significantly. The phase change of the composition samples may originate from the PVP molecular structure. Amide groups in PVP molecules have strong polarity and can easily accept hydrogen bonds. N and O atoms as coordinating atoms lead to the breaking and recombination of chemical bonds and cause a change in the coordination environment of atoms in the crystal lattice of samples. In order to further explore the valence state changes of the V element, the high-resolution V 2p spectra of ZVO, ZVO-0.1P, and ZVO-0.2P are presented in Fig. 1b. It can be clearly observed that the three samples have characteristic peaks of V $2p_{1/2}$ and V $2p_{3/2}$. V $2p_{3/2}$ of ZVO is fitted to two peaks at 517.18 and 517.5 eV, corresponding to species V^{4+} and V^{5+}, respectively [19]. When adding 0.1 g PVP in the synthesis process, the high-resolution V $2p_{3/2}$ of ZVO-0.1P is deconvoluted into two signals located at 515.8 and 517.4 eV, corresponding to V^{3+} and V^{5+}, respectively. When the added amount of PVP is

increased to 0.2 g, the $V2p_{3/2}$ of ZVO-0.2P is reduced to V^{3+} and V^{4+} with binding energy values of 515.6 and 516.97 eV, respectively [26]. The results show that PVP reduces the high-valence state of V to the low-valence state, further indicating that PVP molecules cause a change in the coordination environment of atoms in the crystal lattice of the samples. The hybrid valence of the vanadium-ion centre enhances the electronic conductivity of materials and is beneficial to the multi-step reaction of vanadium during insertion and extraction of Zn^{2+} [27].

In order to investigate the differences in morphology between the three samples, electron microscopy tests were performed as shown in Fig. 2(a–c). Clearly, the three samples have belt-like morphology, but the size uniformity of ZVO is poor. In particular, the agglomeration of the ZVO-0.2P sample is significant. Compared with ZVO and ZVO-0.2P, the dispersion and size uniformity of ZVO-0.1P are improved, which is beneficial for the active material in contact with the electrolyte and contributes to zinc ion free insertion and removal, ensuring good electrochemical performance. The TEM image of ZVO-0.1P (Fig. 2d) further demonstrates that the sample has nanobelt morphology with widths in the range of 100–200 nm. The selected area electron diffraction (SAED) pattern of the sample, depicted in the inset of Fig. 2d, can be well indexed to the crystal pattern, showing a distinct crystalline ring due to the good crystallisation, in agreement with the XRD results.

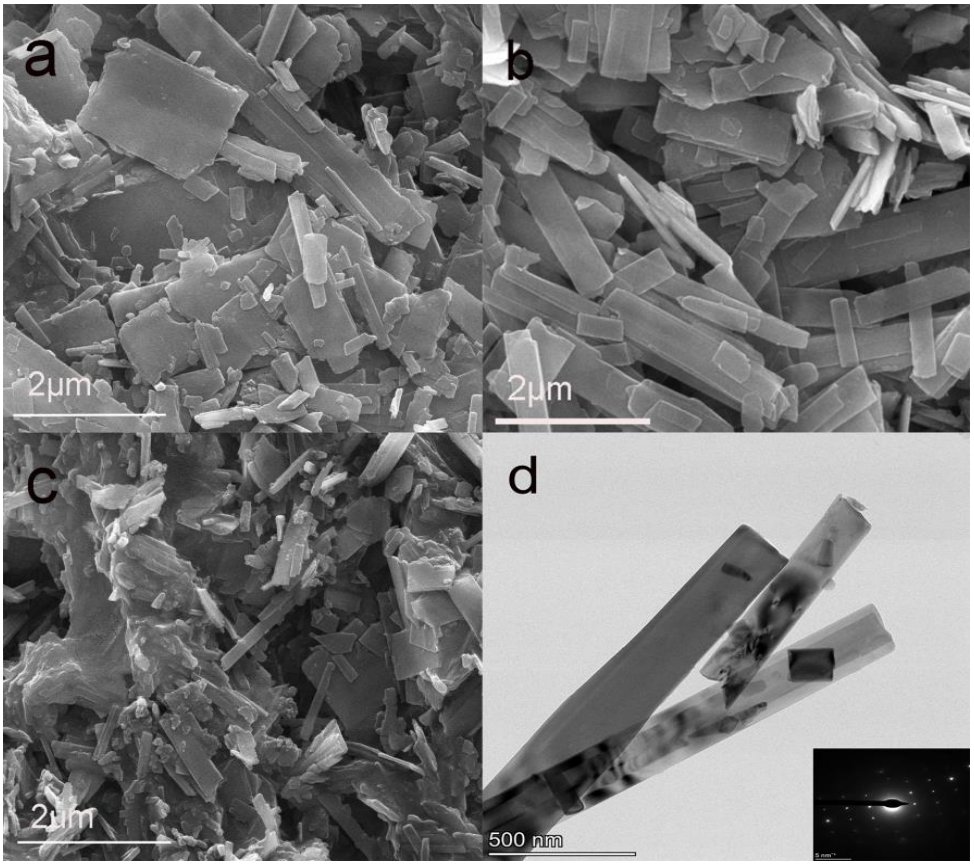

Figure 2. SEM images of ZVO (a), ZVO-0.1P (b), and ZVO-0.2P (c). (d) TEM and SAED (inset) images of ZVO-0.1P.

The electrochemical performances of the ZVO, ZVO-0.1P, and ZVO-0.2P electrodes are shown in Fig. 3. The cycling performances were performed at a current density of 300 mA g^{-1}, as shown in Fig. 3a. Compared with ZVO and ZVO-0.2P, ZVO-0.1P has the highest specific capacities, with an initial discharge capacity of 386 mA h g^{-1}, and remains at 291 mA h g^{-1} after 50 cycles with a Coulombic efficiency of 99.8%, displaying higher reversibility of Zn^{2+} insertion and extraction. More importantly, Fig. 3b shows the rate performance of ZVO, ZVO-0.1P, and ZVO-0.2P at various current densities ranging from 0.05 to 3 A g^{-1}. As a result, the ZVO-0.1P electrode supplies a series of discharge capacities of 348, 336, 289, 260, 224, 160, 112, and 88 mA h g^{-1} at 0.05, 0.1, 0.2, 0.3, 0.5, 1, 2, and 3 A g^{-1}, respectively, which are higher than the discharge capacities for ZVO and ZVO-0.2P. Satisfactorily, even at a large current density of 3 A g^{-1}, the discharge capacity of the ZVO-0.1P electrode remains at 45.7% of 0.5 A g^{-1} (6-fold current density increase), which represents an outstanding rate capability.

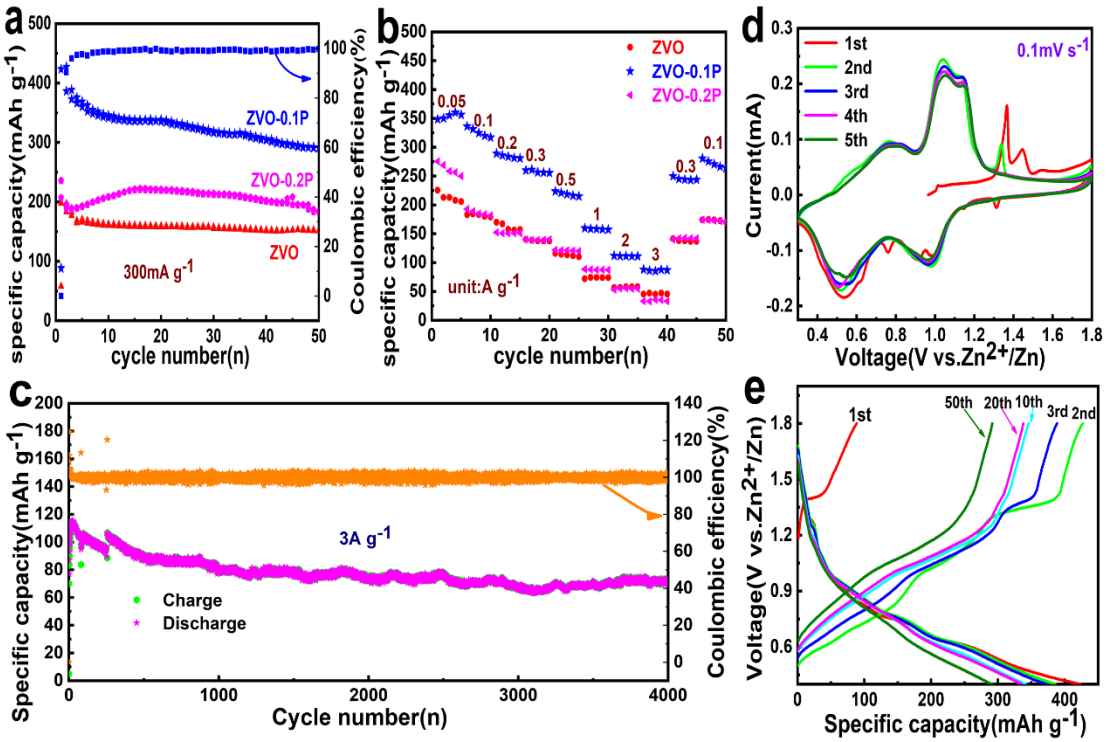

Figure 3. (a) Cycling performances and coulombic efficiencies of ZVO, ZVO-0.1P, and ZVO-0.2P at 300 mA g^{-1}. (b) Rate performance of ZVO, ZVO-0.1P, and ZVO-0.2P at current densities ranging from 0.05 to 3 A g^{-1}. (c) Cycling performance and coulombic efficiency of ZVO-0.1P at 3 A g^{-1}. (d) Cyclic voltammograms of ZVO-0.1P at the scan rate of 0.1 mV s^{-1}. (e) Charge/discharge profiles of ZVO-0.1P at 300 mA g^{-1}.

In particular, when the rate suddenly recovers to 0.3 A g^{-1}, the discharge capacity of 259 mA h g^{-1} can be recovered to a high rate of 96.3%. Finally, in order to further evaluate the stability, the electrode was tested for long-term cycling performance at a current density of 3.0 A g^{-1}, as shown in Fig. 3c. Undergoing an electrode activation process, the ZVO-0.1P electrode displays a maximum capacity of 114 mA h g^{-1}. Meanwhile, a reversible discharge capacity of 64% is obtained after 4000

cycles and a high Coulombic efficiency approaching 100% is maintained, showing an outstanding long-term cycle life. Fig. 3d shows the initial five curves for ZVO-0.1P with a scan rate of 0.1 mV s^{-1}. The curves in the first and second cycles are different from the curves in subsequent cycles. Unlike the last three cycles, the first cycle shows reduction peaks located at 1.37 and 1.45 V and oxidation peaks located at 1.32, 1.00, and 0.91 V, followed by a significant peak at 1.34 V in the second cycle during the reduction process. These anomalous peaks may be attributed to the composite phase of the sample and the occurrence of irreversible reactions [28]. Subordinately, two pairs of redox peaks can be clearly determined at approximately 0.54/1.0 and 0.78/1.1 V, indicating that the reaction mechanism is a multi-step and continuous Zn^{2+} insertion/extraction reaction. In the subsequent three cycles, the CV curves show excellent overlap, confirming that Zn^{2+} insertion/extraction has excellent reversibility and stability. The corresponding charge/discharge profiles of ZVO-0.1P at 300 mA g^{-1} (Fig. 2e) present similar shapes and settled platforms, which are in accordance with the CV curves.

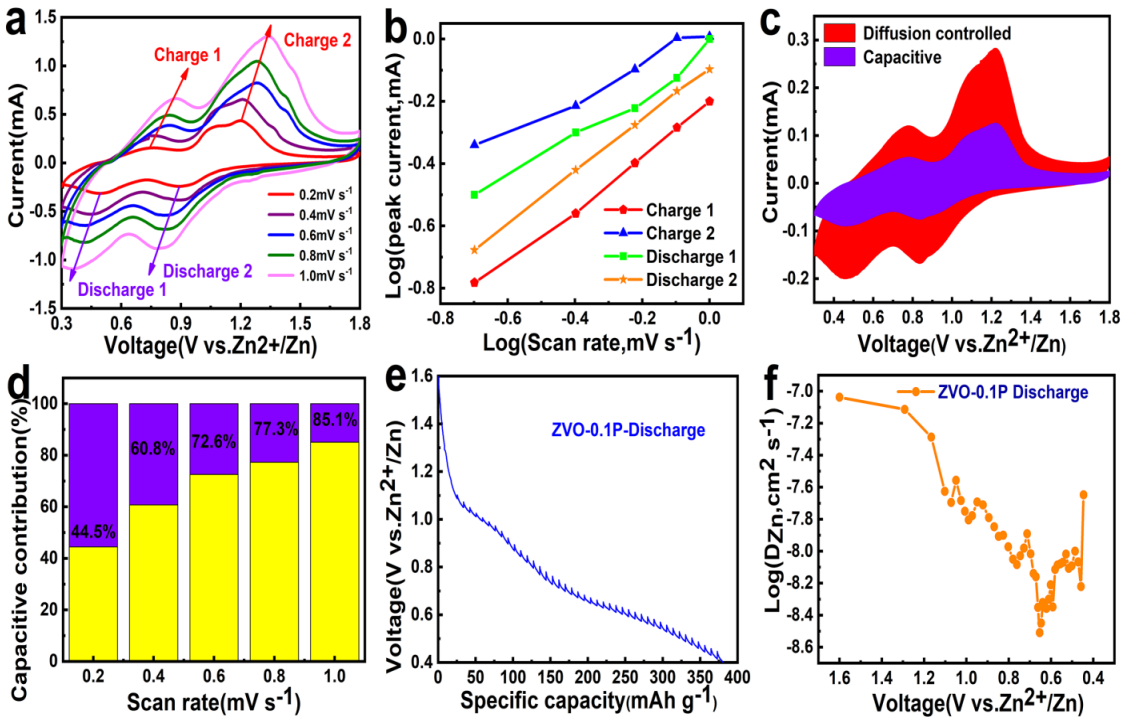

Figure 4. (a) CV curves of ZVO-0.1P electrode at various scanning rates and (b) corresponding plots of log (I)-log (v) at each peak. (c) Capacitive contribution at 0.2 mV s^{-1}. (d) Contribution ratio of capacity-controlled and diffusion-controlled capacities at various scanning rates. Galvanostatic intermittent titration technique (GITT) curves (e) and the corresponding Zn^{2+} diffusion coefficient (f) of ZVO-0.1P for the sixth discharge process.

In view of the excellent electrochemical performance of ZVO-0.1P, to further understand the electrochemical kinetics of the vanadium-based compound composite battery, CV curves were measured at different scan rates ranging from 0.2 to 1.0 mV s^{-1} (Fig. 4a). Markedly, the redox peaks become broader and shift toward higher (oxidation peaks) and lower (reduction peaks) potentials,

which can be attributed to the surface-controlled capacitive and diffusion-controlled processes [29]. The electrochemical kinetics process can be assumed to fit the following equation (1) [30]:

$$i = av^b \quad (1)$$

where i and v are the peak current (mA) and the corresponding scan rate (V s^{-1}), respectively; a and b are variable parameters in which the latter varies in the range of 0.51.0. For a given system, a b-value of 0.5 depicts diffusion-limited processes and a b-value of 1.0 indicates a capacitive process. In the CV curves of ZVO-0.1P with different scanning rates (Fig. 4a), the charge 1, charge 2, discharge 1, and discharge 2 values of ZVO-0.1P are 0.84, 0.54, 0.67, and 0.83, respectively (as shown in Fig. 4b), which means that the electrochemical kinetics of ZVO-0.1P are the result of combining diffusion-control and capacitive-control processes. Furthermore, the contributions of the two processes can be derived according to equation (2) [31]:

$$i = k_1 v + k_2 v^{1/2} \quad (2)$$

where i, $k_1\upsilon$, and $k_2\upsilon^{1/2}$ represent the current response, capacitive, and ionic diffusion contributions, respectively. In Fig. 4a, the capacitive contribution is calculated to be 44.5% at a scan rate of 0.2 mV s^{-1}. With an increase in the scan rate, the percentage of capacitive contribution increases to 60.8%, 72.6%, 77.3%, and 85.1% at scan rates of 0.4, 0.6, 0.8, and 1.0 mV s^{-1}, respectively (Fig. 4d), revealing that the Zn//ZVO-0.1P batteries have favourable charge transfer kinetics.

To better understand the kinetics during the diffusion of Zn^{2+} ions in the ZVO-0.1P electrode, galvanostatic intermittent titration technique (GITT) measurements were carried out to determine the average diffusion coefficient around the redox peaks. The GITT data were collected at a current density of 100 mA g^{-1} for 10 min and a rest interval of 20 min (Fig. 4e). The ionic diffusion coefficient in the ZVO-0.1P electrode as a function of voltage can be determined by the following equation (3) [32]:

$$D = \frac{4}{\pi\tau}\left(\frac{m_B V_M}{M_B S}\right)\left(\frac{\Delta E_S}{\Delta E_\tau}\right) \quad (3)$$

where τ is the constant current pulse time; m_B, Vm, M_B, and S represents the mass loading in the electrode, the molar volume of ZVO-0.1P, the molecular weight of ZVO-0.1P, and the surface area of the electrode, respectively. ΔE_S and $\Delta E\tau$ represent the change in the equilibrium potential and the total change in cell voltage during the current pulse, respectively. The ion diffusion coefficient of ZVO-0.1P strongly depends on the discharge process [21]. The average D value of the ZVO-0.1P electrode was calculated to be approximately 1.36×10^{-8} for the sixth discharge process (Fig. 4f), indicating fast Zn^{2+} diffusion kinetics, which can be responsible for the remarkable electrochemical performance of ZVO-0.1P.

4. CONCLUSIONS

In summary, we propose aqueous rechargeable ZIBs based on the vanadium-based compound composite cathode and zinc anode. Vanadium-based compound composites consisting of $Zn_2V_2O_7$, ZnV_2O_6, and ZnV_2O_4 are prepared via a facile hydrothermal method using PVP as the regulator. PVP

causes the phase change of samples, improves dispersion, and reduces the high-valence state of V to the low-valence state. The good dispersion and hybrid valence of the vanadium-based compound composite are helpful for the electrochemical performance. ZVO-0.1P displayed an initial discharge capacity of 386 mA h g^{-1} and retained 291 mA h g^{-1} after 50 cycles with a Coulombic efficiency of 99.8%. At 3 A g^{-1}, undergoing an electrode activation process, the ZVO-0.1P electrode displayed a maximum capacity of 114 mA h g^{-1}. Meanwhile, a reversible discharge capacity of 64% was obtained after 4000 cycles and high Coulombic efficiency was maintained, showing an outstanding long-term cycle life. The electrochemical kinetics of ZVO-0.1P are the result of combining the diffusion-control and capacitive-control processes. The average D value of the ZVO-0.1P electrode was calculated to be approximately 1.36×10^{-8} for the sixth discharge process, indicating fast Zn^{2+} diffusion kinetics.

ACKNOWLEDGEMENTS
This work was supported by the Opening Project of Guangxi Key Laboratory of Green Processing of Sugar Resources (No. GXTZY202004), the Natural Science Key Foundation of Guangxi Province (No. 2019GXNSFDA245025), High Levels of Innovation Team and Excellence Scholars Program in Colleges of Guangxi, and the Research Foundation for the Doctoral Program of Guangxi University of Science and Technology (No.16Z02).

References

1. L. M. Suo, O. Borodin, T. Gao, M. Olguin, J. Ho, X. L. Fan, C. Luo, C. S. Wang and K. Xu, *Science*, 350 (2015) 938.
2. Y. Zhao, X. F. Li, B. Yan, D. B. Xiong, D. J. Li, S. Lawes and X. L. Sun, *Adv. Energy Mater.*, 6 (2016).
3. W. W. Zhang, C. Tang, B. X. Lan, L. N. Chen, W. Tang, C. L. Zuo, S. J. Dong, Q. Y. An and P. Luo, *J. Alloy Compd.*, 819 (2020).
4. H. Tang, Z. Peng, L. Wu, F. Y. Xiong, C. Y. Pei, Q. Y. An and L. Q. Mai, *Electrochem Energy R*, 1 (2018) 169.
5. X. S. Tao, Q. Zhang, Y. Li, X. L. Lv, D. L. Ma and H. G. Wang, *Appl. Surf. Sci.*, 490 (2019) 47.
6. N. Nitta, F. Wu, J. T. Lee and G. Yushin, *Mater. Today*, 18 (2015) 252.
7. D. Miranda, C. M. Costa and S. Lanceros-Mendez, *J. Electroanal. Chemistry*, 739 (2015) 97.
8. M. Song, H. Tan, D. L. Chao and H. J. Fan, *Adv. Funct. Mater.*, 28 (2018).
9. F. Tang, W. Zhou, M. Chen, J. Chen and J. Xu, *Electrochimica Acta*, 328 (2019) 135137.
10. Y. Liu and X. Wu, *J. Energy Chem.*, 56 (2021) 223.
11. X. Jia, C. Liu, Z. G. Neale, J. Yang and G. Cao, *Chem. Rev.*, 120 (2020) 7795.
12. G. Kasiri, J. Glenneberg, R. Kun, G. Zampardi and F. La Mantia, *ChemElectroChem*, 7 (2020) 3301.
13. H. Fei, *Int. J. Electrochem. Sci.*, 14 (2019) 11560.
14. Y. Yang, X. Chuan, J. Li, F. Liu and A. Li, *Int. J. Electrochem. Sci.*, 15 (2020) 6052.
15. S. Wu, Y. Ding, L. Hu, X. Zhang, Y. Huang and S. Chen, *Mater. Lett.*, 277 (2020) 128268.
16. B. Tang, J. Zhou, G. Fang, S. Guo, X. Guo, L. Shan, Y. Tang and S. Liang, *J. Electrochem. Soc.*, 166 (2019) A480.
17. D. Kundu, B. D. Adams, V. Duffort, S. H. Vajargah and L. F. Nazar, *Nat. Energy*, 1 (2016).
18. Y. Yang, Y. Tang, S. Liang, Z. Wu, G. Fang, X. Cao, C. Wang, T. Lin, A. Pan and J. Zhou, *Nano Energy*, 61 (2019) 617.
19. F. Ming, H. Liang, Y. Lei, S. Kandambeth, M. Eddaoudi and H. N. Alshareef, *ACS Energy Lett.*, 3 (2018) 2602.
20. F. Hu, D. Xie, F. Cui, D. Zhang and G. Song, *RSC Adv.*, 9 (2019) 20549.

21. F. Hu, D. Xie, D. Zhao, G. Song and K. Zhu, *J. Energy Chem.*, 38 (2019) 185.
22. P. Hu, T. Zhu, X. Wang, X. Wei, M. Yan, J. Li, W. Luo, W. Yang, W. Zhang, L. Zhou, Z. Zhou and L. Mai, *Nano lett.*, 18 (2018) 1758.
23. J. G. Chuan Xia, Yongjiu Lei, Hanfeng Liang, Chao Zhao, and Husam N. Alshareef, *Adv. Mater.*, 30 (2018) 1705580.
24. B. Sambandam, V. Soundharrajan, S. Kim, M. H. Alfaruqi, J. Jo, S. Kim, V. Mathew, Y.-k. Sun and J. Kim, *J. Mater. Chem. A*, 6 (2018) 3850.
25. Y. Liu, C. Li, J. Xu, M. Ou, C. Fang, S. Sun, Y. Qiu, J. Peng, G. Lu, Q. Li, J. Han and Y. Huang, *Nano Energy*, 67 (2020) 104211.
26. R. Wei, X. Wang, B. Xi, Z. Feng, H. Li, W. Chen, Y. Jia, J. Feng and S. Xiong, *ACS Appl. Energy Mater.*, 3 (2020) 5343.
27. Z. Wu, Y. Wang, L. Zhang, L. Jiang, W. Tian, C. Cai, J. Price, Q. Gu and L. Hu, *ACS Appl. Energy Mater.*, 3 (2020) 3919.
28. D. L. Chao, C. Zhu, M. Song, P. Liang, X. Zhang, N. H. Tiep, H. F. Zhao, J. Wang, R. M. Wang, H. Zhang and H. J. Fan, *Adv. Mater.*, 30 (2018).
29. W. Tang, B. X. Lan, C. Tang, Q. Y. An, L. N. Chen, W. W. Zhang, C. L. Zuo, S. J. Dong and P. Luo, *ACS Sustain Chem. Eng.*, 8 (2020) 3681.
30. F. Hu, D. Xie, F. H. Cui, D. X. Zhang and G. H. Song, *RSC Adv.*, 9 (2019) 20549.
31. F. Wan, L. L. Zhang, X. Dai, X. Y. Wang, Z. Q. Niu and J. Chen, *Nat. Commun.*, 9 (2018).
32. Y. Y. Liu, Q. Li, K. X. Ma, G. Z. Yang and C. X. Wang, *ACS Nano*, 13 (2019) 12081.